Translational Oncology
www.transonc.com

Volume 8 Number 6 December 2015 pp. 446–455 446

Association of Diffusion and Anatomic Imaging Parameters with Survival for Patients with Newly Diagnosed Glioblastoma Participating in Two Different Clinical Trials[1]

Qiuting Wen*†,2, Laleh Jalilian*2, Janine M. Lupo*, Yan Li*, Ritu Roy§,¶, Annette M. Molinaro§,¶, Susan M. Chang§, Michael Prados§, Nicholas Butowski§, Jennifer Clarke§ and Sarah J. Nelson*†,‡

*Department of Radiology and Biomedical Imaging, University of California, San Francisco, San Francisco, CA United States; †UCSF/UCB Joint Graduate Group in Bioengineering, University of California, San Francisco, San Francisco, CA United States; ‡Department of Bioengineering and Therapeutic Sciences, University of California, San Francisco, San Francisco, CA United States; §Department of Neurological Surgery, University of California, San Francisco, San Francisco, CA United States; ¶Department of Epidemiology and Biostatistics, University of California, San Francisco, San Francisco, CA United States

Abstract

PURPOSE: To evaluate the time course and association with survival of anatomic lesion volumes and diffusion imaging parameters for patients with newly diagnosed glioblastoma who were treated with radiation and concurrently with either temozolomide and enzastaurin (TMZ+enza cohort) or temozolomide, erlotonib, and bevaciumab (TMZ+erl+bev cohort). *MATERIALS AND METHODS:* Regions of interest corresponding to the contrast-enhancing and hyperintense lesions on T2-weighted images were generated. Diffusion-weighted images were processed to provide maps of apparent diffusion coefficient, fractional anisotropy, and longitudinal and radial eigenvalues. Histograms of diffusion values were generated and summary statistics calculated. Cox proportional hazards models were employed to assess the association of representative imaging parameters with survival with adjustments for age, Karnofsky performance status, and extent of resection. *RESULTS:* Although progression-free survival was significantly longer for the TMZ+erl+bev cohort (12.8 vs 7.3 months), there was no significant difference in overall survival between the two populations (17.0 vs 17.8 months). The median contrast-enhancing lesion volumes decreased from 6.3 to 1.9 cm^3 from baseline to the postradiotherapy scan for patients in the TMZ+enza cohort and from 2.8 to 0.9cm^3 for the TMZ+erl+bev cohort. Changes in the T2 lesion volumes were only significant for the latter cohort (26.5 to 11.9 cm^3). The median apparent diffusion coefficient and related diffusion parameters were significantly increased for the TMZ+enza cohort (1054 to 1225 $\mu m^2/s$). More of the anatomic parameters were associated with survival for the TMZ+enza cohort, whereas more diffusion parameters were associated with survival for the TMZ+erl+bev cohort. *CONCLUSION:* The early changes in anatomic and diffusion imaging parameters and their association with survival reflected differences in the mechanisms of action of the treatments that were being given. This suggests that integrating diffusion metrics and anatomic lesion

Address all correspondence to: Sarah J. Nelson, PhD, Department of Radiology and Biomedical Imaging, UCSF, 1700 4th St, Byers Hall, Box 0775, UCSF, San Francisco, CA 94143-0775.
E-mail: sarah.nelson@ucsf.edu

[1]Grant support: This work was supported by grants R01 CA127612 and P01 CA118816 from the National Institutes of Health.

[2]These authors contributed equally to this work.

Received 12 June 2015; Revised 14 September 2015; Accepted 2 October 2015

1936-5233/15
http://dx.doi.org/10.1016/j.tranon.2015.10.001

volumes into the Response Assessment in Neuro-Oncology criteria would assist in interpreting treatment-induced changes and predicting outcome in patients with newly diagnosed glioblastoma who are receiving such combination treatments.

Translational Oncology (2015) 8, 446–455

Introduction

Glioblastoma (GBM) is the most malignant primary malignant brain tumor in adults. The standard of care for patients with newly diagnosed GBM consists of surgery, radiotherapy (RT), and temozolomide (TMZ). In a recent phase III trial, patients treated in this manner had significantly improved overall survival (OS) compared with patients who received RT alone [1]. The median overall survival obtained with this treatment was 15 months [1]. A number of different therapeutic agents that are expected to have a synergistic effect with RT and TMZ have been considered [2–6], with the goal of improving outcomes for patients with GBM. Assessment of early response to these combination treatments is complicated by their different mechanisms of action and the impact that they have on standard magnetic resonance (MR) imaging parameters [7].

Enzastaurin is a protein kinase C β-inhibitor that is reported as having a direct antitumor effect through the suppression of tumor cell proliferation and induction of apoptosis, and indirect effects that are expressed by the inhibition of tumor-induced angiogenesis [8]. Preclinical reports have shown that it is synergistic with radiation and induces apoptosis in glioma model systems [9]. These data provided the rationale for a recent phase II clinical trial of RT, TMZ, and enzastaurin in patients with newly diagnosed GBM. Although the clinical outcome data for patients from this study have already been reported [3], the role of advanced imaging parameters in assessing efficacy and predicting outcome has not yet been presented.

Another agent of interest for combination therapy is bevacizumab, which is a humanized monoclonal vascular endothelial growth factor (VEGF)–blocking antibody that normalizes vascular permeability and regulates angiogenesis [10]. Preliminary studies of bevacizumab in patients with recurrent GBM have shown a dramatic decrease in the size of the enhancing lesion and an increase in progression-free survival (PFS) [11–13]. This led to a number of clinical trials of patients with GBM that combined bevacizumab with standard RT and chemotherapy. The biological hypotheses that have driven these analyses are that combination treatment would normalize tortuous tumor vasculature, improve the delivery of chemotherapeutics, and hence provide improved overall survival [14].

The disadvantage of treatments such as enzastaurin and bevacizumab is that they cause changes in anatomic imaging characteristics, which can make it difficult to use conventional methods for assessing response to therapy. For example, agents that reduce proliferation may result in a clinical assessment of stable disease, whereas antiangiogenic agents decrease the size of the contrast-enhancing lesion (CEL), but this does not necessarily signify a reduction in bulk tumor [11]. Another complication of anti-VEGF agents that have been reported is to result in increased tumor invasiveness that is expressed by an increase in the size of the region of T2 hyperintensity rather than the changes in the enhancing lesions [15]. Although the Response Assessment in Neuro-Oncology criteria include consideration of changes in the T2 lesion as part of the definition of response to therapy [16], it is not clear whether such changes are specific to recurrent tumor or represent nonspecific RT-induced changes in normal white matter.

Diffusion-weighted imaging has been proposed as an adjunct to standard anatomic imaging because it can provide new information about response to therapy through the evaluation of parametric images that reflect variations in tissue composition and architecture [17–19]. The most widely considered variable is the apparent diffusion coefficient (ADC), which is sensitive to an increase in tumor cellularity, formation of necrosis, and the presence of vasogenic edema. Other variables of interest are the fractional anisotropy (FA), which describes variability in the directionality of diffusion, and eigenvalues (EV1 and EVrad), which provide information on the magnitude of the preferred (longitudinal) direction of diffusion and average perpendicular components. These reflect local variations in tissue properties associated with unregulated cell growth and changes in the extracellular environment. The hypotheses of interest are that a decrease in FA reflects breakdown of normal brain structure and that the magnitude of EV1 and EVRAD may be more sensitive to such changes than the ADC alone.

Metrics describing pretreatment and early changes in diffusion within the CEL have been reported as predictors of response to therapy in brain tumors [17–22]. These include the evaluation of histograms of ADC at single time points [20,21] and the functional diffusion map (fDM), which describes changes between ADC values on a pixel-by-pixel basis in overlapping regions of the CEL from two successive scans [17,18]. Although these methods have been applied to the assessment of agents such as bevacizumab [19,22], the relatively small size of the CEL in follow-up scans means that they do not meet the cutoff criterion of 3 to 4 cm^3 that was originally defined for this type of analysis [17,18].

The purpose of this study was to compare the patterns of early changes in anatomic and diffusion parameters for patients with newly diagnosed GBM who had received advanced imaging examinations and had been participating in two different clinical trials. The hypothesis was that the metrics considered would provide information about the effectiveness of the treatments being considered. Scans were obtained at baseline and at three follow-up time points. Imaging parameters derived from these scans were evaluated to see if they were associated with PFS and OS.

Methods

Study+ Population

A total of 75 patients with newly diagnosed GBM (WHO grade IV) who had received advanced imaging examinations and had participated in phase II clinical trials at UCSF were evaluated in this study. Their diagnosis was based upon histological analysis of tissue from surgical

Table 1. Summary of Patient Characteristics for the Two Cohorts

	Total # Patients	Total # Scans	Age	Gender	Extent of Resection			KPS
			Median (Range)	M/F	Biopsy	Subtotal	Gross Total	Range
TMZ+enza	44	133	57 (25-80)	32/12	7	27	10	60-90
TMZ+erl+bev	31	103	52 (21-76)	15/16	5	17	9	60-100

samples using the WHO criteria. After surgery, 44 of the patients were treated with standard care of RT and concurrent TMZ in conjunction with enzastaurin (TMZ+enza cohort), and 31 of the patients were treated with erlotinib and bevacizumab (TMZ+erl+bev cohort). Patients were required to have a Karnofsky performance score (KPS) of ≥ 60 and to provide informed consent as approved by the Committee on Human Research at UCSF. Patient characteristics were summarized in Table 1.

The treatment schemas are represented in Figure 1 and have been described in prior publications describing the clinical results of the trials [3,4]. Briefly, they began within 5 weeks of diagnosis with fractionated RT (total dose of 60 Gy) and 75 mg/m^2 of TMZ given daily over a period of 6 weeks. Patients in the TMZ+enza cohort were administered enzastaurin (250 mg daily) concurrently with TMZ. Patients in the TMZ+erl+bev cohort received erlotinib (patients not on antiepileptic drugs received 150 mg/day continuously and patients on antiepileptic drugs received 500 mg/day continuously) starting on day 1 of RT and bevacizumab at a dose of 10 mg/kg IV every 14 days starting in week 2 of radiotherapy. MR exams considered in the analysis were performed at four time points: following surgical resection but before RT (baseline/pre-RT), between 3 and 5 weeks into treatment (1 month/mid-RT), within 2 weeks after completion of RT (2 months/post-RT), and at the next follow-up scan (4 months).

Criteria that had been used to define true progression were clinical deterioration and/or radiological progression, which were based upon visual assessment of changes in cross-sectional diameters of the CEL as defined by the McDonald criteria for the TMZ+enza cohort [23] and by the Response Assessment in Neuro-Oncology criteria for the TMZ+erl+bev cohort. The latter integrates changes in the T2-hyperintensity lesion into the definition of response [16]. When tumor progression was suspected, patients had received an additional clinical scan at a short time interval (~ 1 month) to help in distinguishing true progression from pseudoprogression.

MR Imaging and Postprocessing

A total of 239 scans were considered in the analysis, 133 from the TMZ+enza cohort and 106 from the TMZ+erl+bev cohort. All of the scans were obtained using a 3-T MR scanner (General Electric Medical Systems) using the body coil for transmission and an eight-channel phased array coil for reception. The examination included axial T2-weighted fluid attenuated inversion recovery (FLAIR) images, volumetric T1-weighted inversion recovery spoiled gradient echo images obtained pre- and postinjection of the contrast agent gadopentetate dimeglumine, and six-directional axial diffusion-weighted imaging (DWI) (b = 1000 s/mm^2, number of excitations = 4) sequences.

The FLAIR and precontrast T1-weighted images were rigidly aligned to the postcontrast T1-weighted images using previously developed software [24]. The T2 lesions were segmented based on the hyperintensity region of FLAIR images using a semiautomatic method [25]. Contrast-enhancing (CE) lesions were manually defined on the co-registered post-Gad T1 SPGR images at each available time point. Any enhancement that was also present on the precontrast T1 images was assumed to be indicative of acute blood products and was excluded. To aid in performing this analysis, T1-subtraction (T1S) images were calculated by weighting the intensities in the pre-Gad images by the ratio of the intensities in normal-appearing white matter for the post- versus the pre-Gad images and then subtracting them from the corresponding post-Gad images [26]. The T1S lesion was identified by thresholding the corresponding image within the T2 lesion at a level of 0.2 times the median intensity in normal-appearing white matter of the postcontrast image. This threshold was chosen empirically to represent areas that were in good visual agreement with the CEL. The resection cavity was excluded from all regions of interest.

ADC, FA, EV1, and EVrad values were calculated on a voxel-by-voxel basis using software that was developed in-house and based on previously published algorithms [27]. The values obtained were related to regions of interest on anatomical imaging by rigidly aligning the T2-weighted (b = 0) diffusion image to the T2-weighted FLAIR and applying the transformation to the ADC maps. Figure 2 shows an example of the CE and T2 lesion regions of interest superimposed upon aligned images from baseline, mid-RT, and post-RT scans.

Statistical Analysis

The volumes of the CE, T1S, and T2 lesions were obtained by counting the number of pixels in each region and multiplying by the pixel dimensions. Histograms of diffusion values were obtained from within the T2 lesion. Parameters that were used to summarize the shape of the histograms at individual time points were the median, 10th, 25th, 75th, and 90th percentile of the distribution. The changes in volumes and diffusion parameter values relative to the baseline scan for subjects within each cohort were evaluated using a Wilcoxon signed rank test. Differences in imaging parameters between the two cohorts were evaluated using a Wilcoxon rank sum test.

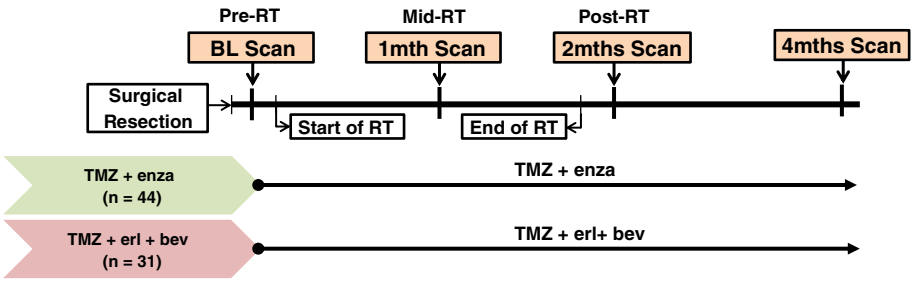

Figure 1. Treatment schemes for the two patient cohorts considered in this study.

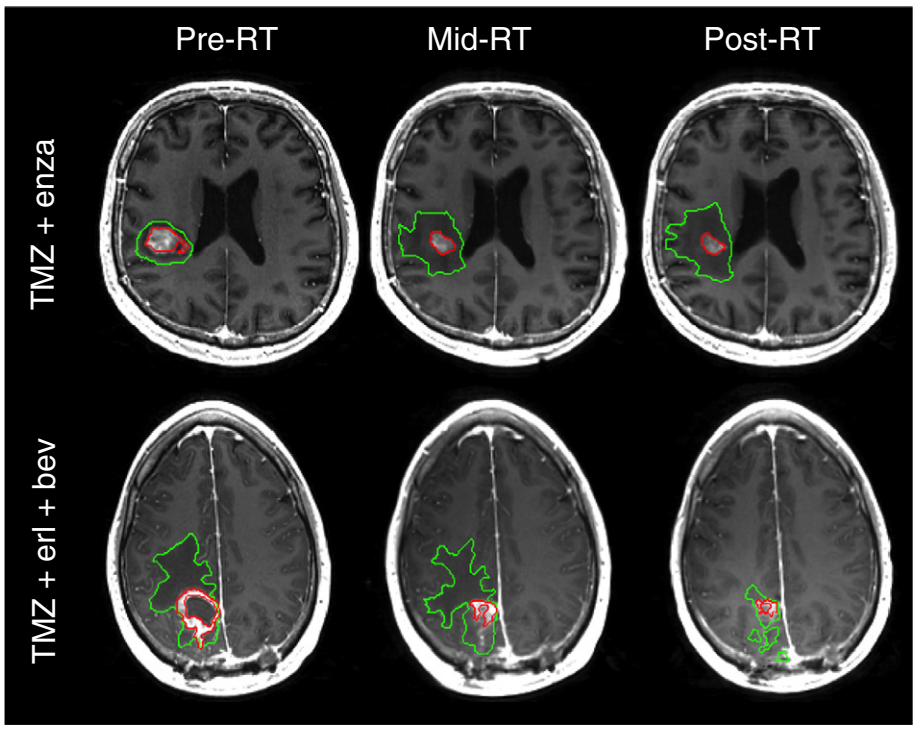

Figure 2. CEL (red) and T2L (green) regions of interest superimposed upon aligned T1-weighted postcontrast images from baseline, mid-RT, and post-RT scans.

Survival Analysis

OS and PFS were evaluated using Kaplan-Meier survival curves. The log-rank test was used to compare the variables among patient cohorts. OS was determined from the day of the baseline scan to the date of death or last contact at which the patient was known to be alive (censored). PFS was defined as the time from the baseline scan to disease progression or death due to any cause, whichever came first.

Association of Imaging Parameters and Outcome

Cox proportional hazard models were used to evaluate which parameters were associated with PFS or OS within each treatment cohort. In this analysis, adjustments were made for clinical factors of baseline KPS, age, and extent of resection (0 = biopsy, 1 = subtotal, 2 = gross total). Multivariate Cox hazard models were considered with covariates for treatment cohort, imaging parameter, and the interaction between treatment cohort and imaging variable. To be considered for multivariate analysis, imaging parameters needed to first show significance on a univariate basis. No formal adjustment of type I error was undertaken because of the exploratory nature of the study. *P* values less than .05 were considered significant. The statistical analyses were performed with RStudio (Version 0.98.953, RStudio, Inc.).

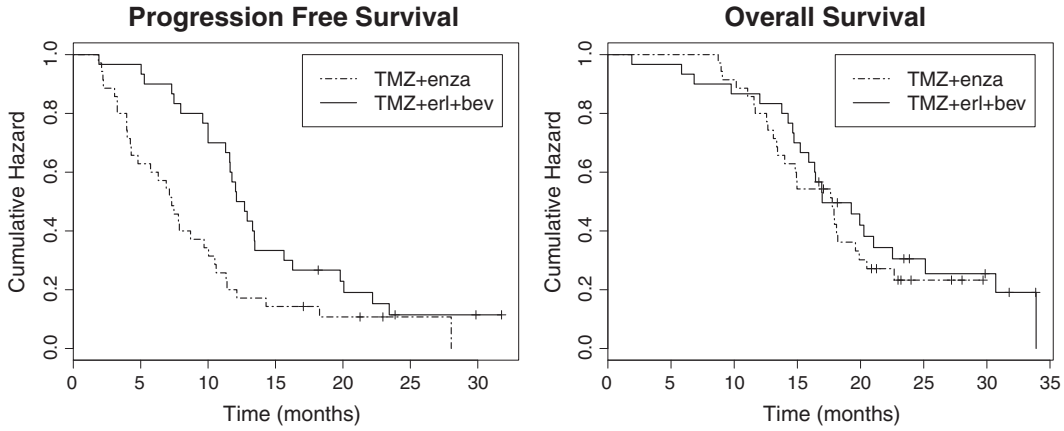

Figure 3. The Kaplan-Meier curves of PFS and OS for the 44 patients in the TMZ+enza cohort and the 31 patients in the TMZ+erl+bev cohort. Median PFS values were 7.3 months and 12.4 months, whereas median OS values were 17.8 months and 17.0 months, respectively. Log-rank tests showed that PFS was significantly longer in the TMZ+erl+bev cohort but that there was no significant difference in OS between the two patient cohorts.

Table 2. Volumes of Anatomic Regions of Interest for All Subjects

		TMZ+enza Cohort				TMZ+erl+bev Cohort			
Timepoint		Baseline	1 mth	2 mths	4 mths	Baseline	1 mth	2 mths	4 mths
# Subjects		39	29	38	27	29	25	25	27
T2 volume (cm^3)	median	20.6	22.4	18.5	17.6	26.5	24.2	10.4*	11.9*
	min	3.5	4.9	3.4	4.2	1.7	2.3	0.1	0.3
	max	115.9	78.8	88.3	157.9	142.3	139.2	42.8	43.5
CE volume (cm^3)	median	6.3	4.1*	3.3*	1.9*	2.8	1.2*	0.7*	0.2*
	min	0.0	0.6	0.0	0.0	0.0	0.0	0.0	0.0
	max	29.6	19.1	29.5	20.8	21.9	17.6	8.7	3.5
T1S volume (cm^3)	median	7.3	5.2*	4.0*	2.8*	6.3	3.7*	1.1*	0.9*
	min	2.7	1.7	0.7	0.1	0.0	0.0	0.0	0.0
	max	52.6	20.5	37.3	74.6	37.9	29.9	8.7	7.6

The asterisk denotes circumstances for which the change in volume from the baseline (pre-RT) value was significant based upon a Wilcoxon signed rank test.

Results

Patients Characteristics and Outcomes

Age, KPS, and extent of resection were not significantly different amongst the two patient cohorts ($P > .1$). Kaplan-Meier curves describing PFS and OS are displayed in Figure 3. Median PFS was 7.3 months in the TMZ+enza cohort (95% confidence interval [CI]: 4.89-10.5 months) and 12.4 months in the TMZ+erl+bev cohort (95% CI: 11.60-16.3 months). Median OS was 17.8 months in the TMZ+enza cohort (95% CI: 14.0-20.5 months) and 17.0 months in the TMZ+erl+bev cohort (95% CI: 15.9-25.1 months). Although the PFS was significantly longer for the TMZ+erl+bev cohort (log-rank test, $P < .008$), there was no significant difference in OS between the two groups ($P > .1$).

Temporal Changes in Anatomic Lesion Volumes

Table 2 shows the changes in volumes of the T2, CE, and T1S lesions as a function of time for the two cohorts. The majority of patients in the TMZ+erl+bev cohort had a marked, significant decrease in the volume of the T2 lesion from pre- to post-RT from a median of 26.6 cm^3 to 10.4 cm^3 ($P < .0001$), whereas the patients in the TMZ+enza cohort had median T2 volumes of 20.6 cm^3 at the pre-RT and 18.5 cm^3 at the post-RT scan ($P = .1645$). The reductions in the CEL volumes for the TMZ+erl+bev cohort were from a median of 2.8 cm^3 to 0.7 cm^3 ($P < .0001$) and for the TMZ+enza cohort from 6.3 cm^3 to 3.3 cm^3 ($P = .0054$). When viewed as a percentage reduction, the magnitude of the decrease was significantly larger for the TMZ+erl+bev cohort (median of −79% versus a median of −39%; $P < .001$).

Figure 4 shows a representation of the variability in volumes of the CEL on a per patient basis for subjects who had data at all four time points. It is clear that, for many of the patients, either the initial or follow-up CE volumes were substantially reduced in size. For the TMZ+erl+bev cohort, the percentage of subjects with CEL volume less than 3 cm^3 at the pre-RT exam was 52%, increasing to 64%, 76%, and 89% at follow-up examinations. For the TMZ+enza cohort, the corresponding changes were from 18% to 31%, 39%, and 59%. The lesions were typically irregular in shape and often formed a narrow rim around the surgical cavity. Figure 5 shows an example of the baseline anatomic images from one such subject, together with bar graphs of the median volumes of the CE, T2, and T1S lesions. These show the relative sizes of the lesions and the pattern of changes at different time points. Although the median T1S lesion volumes were slightly larger than the manually defined CEL volumes, they showed similar patterns of changes and were still relatively small for follow-up scans.

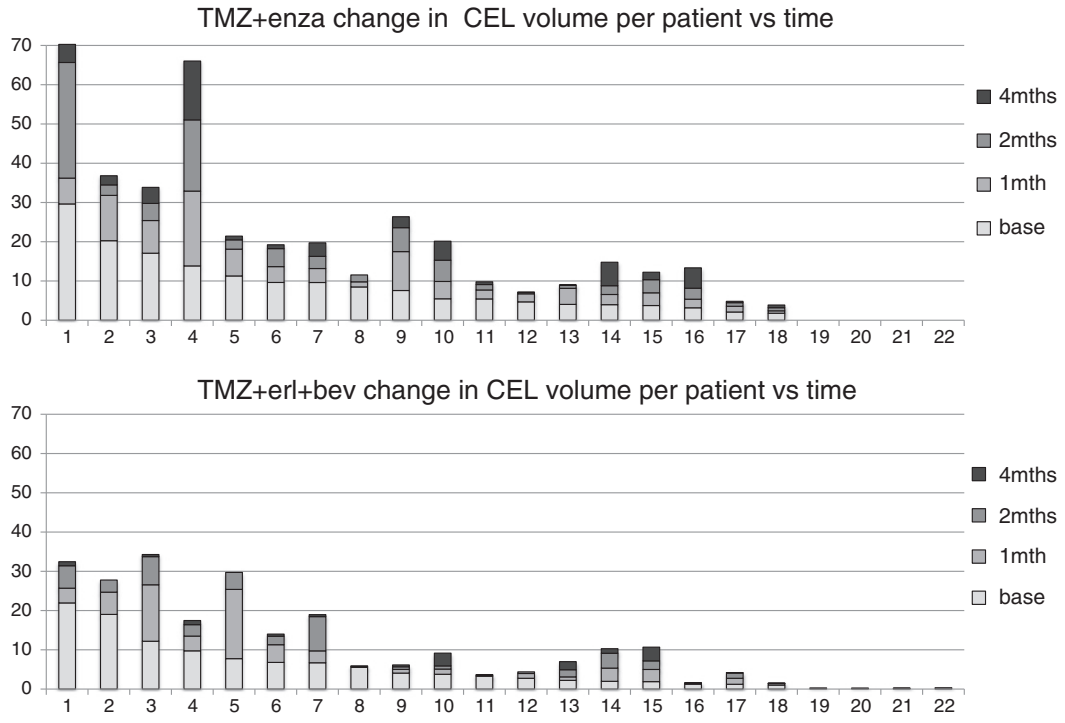

Figure 4. Changes in CEL volume on a per patient basis for the subjects in each cohort who had data from all four time points. This shows that there was considerable variability in lesion volumes but that, in many cases, volumes at follow-up scans were less than 2 to 3 cm^3 in size.

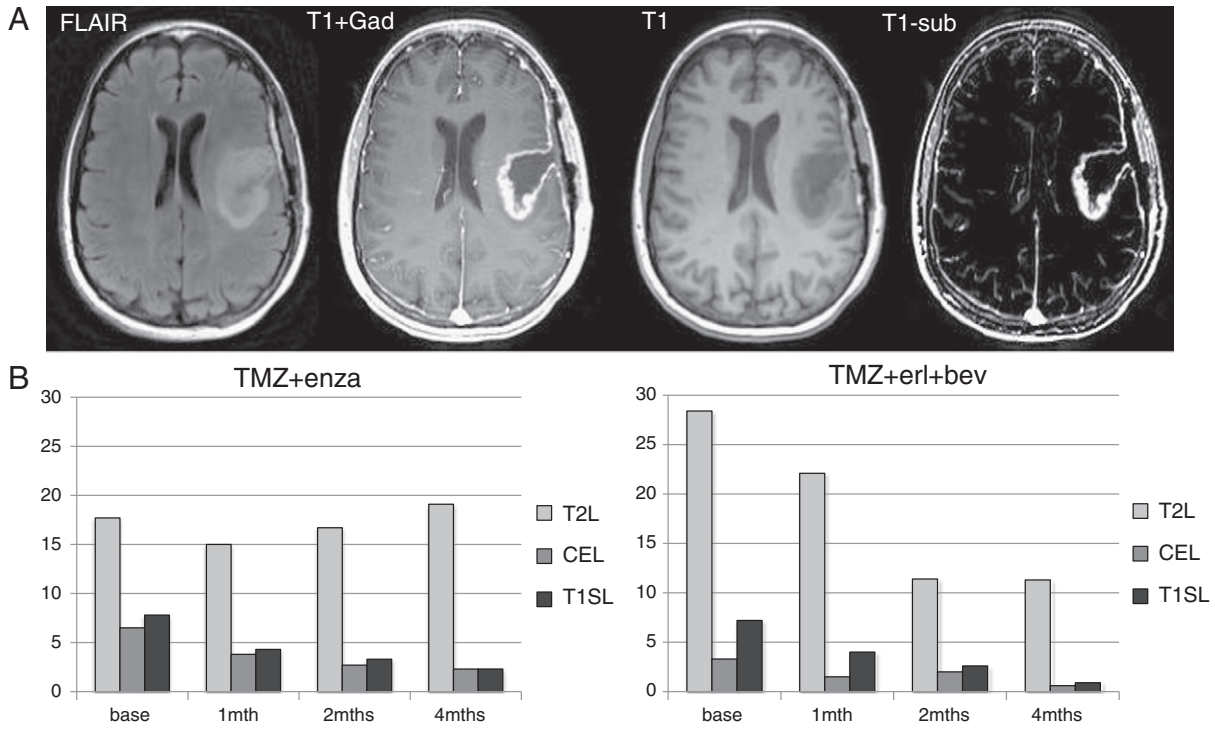

Figure 5. The images in (A) show baseline FLAIR, T1-Gad, T1, and T1S images from one subject. The bar plots in (B) show the time course of changes in median volumes of the CE, T2, and T1S lesions for patients with all four scans. These show the differences in lesion volumes and the patterns of changes in follow-up scans.

Because of the challenges inherent in comparing variations in image intensity parameters within regions of interest that were as small as the CE and T1S lesion volumes, the analysis of diffusion parameters in this study focused on values within the T2 lesion. The median, 25th percentile, and 10th percentile ADC values within the T2 lesion for all patients that were studied at each time point are seen in Table 3. For the TMZ+enza cohort, there were significant increases in ADC intensity metrics from the baseline to 1-, 2-, and 4-month follow-up scans. Although there was a general trend toward decreasing ADC values for the TMZ+erl+bev cohort, the changes from baseline were not significant. These differences are clearly seen in Figure 6, which shows an example of diffusion maps from the baseline scan in the patient shown previously and changes in median, 25th, and 10th percentile for patients in the two cohorts who had scans at all four time points. Similar trends were seen for the other diffusion intensity parameters (EV1 and EVrad).

To obtain estimates of changes in the volumes of regions within the T2 lesion that had low ADC values, cutoffs of 900, 1000, and 1200 $\mu m^2/s$

Table 3. ADC Metrics in Units of $\mu m^2/s$ at Each Time Point of All Subjects With Diffusion Data

		TMZ+enza Cohort				TMZ+erl+bev Cohort			
Time Point		Baseline	1 Mth	2 Mths	4 Mths	Baseline	1 Mth	2 Mths	4 Mths
# Subjects		39	29	38	27	29	25	25	27
ADC median	Median	1054	1158*	1225*	1225*	1174	1134	1074	1044
	Min	825	875	835	925	893	1005	825	805
	Max	1578	1675	1755	1448	1608	1615	1918	1525
ADC 25%	Median	895	1015*	1065*	1080*	1012	985	934	934
	Min	415	755	198	835	773	875	745	705
	Max	1413	1218	1315	1303	1388	1375	1918	1305
ADC10%	Median	775	903*	945*	965*	902	875	824	835
	Min	253	665	138	765	605	698	675	595
	Max	1233	1063	1145	1148	1148	1135	1918	1065
Vol (ADC < 1200) in T2 lesion (cm^3)	Median	9.1	8.6*	7.7	6.2	7.1	14.4	6.1*	6.3*
	Min	0.8	1.1	0.6	1.2	0.6	0.4	0.6	0.3
	Max	60.2	39.9	48.4	125.4	61.7	51.1	29.4	30.4
Vol (ADC < 1000) in T2 lesion (cm^3)	Median	5.4	3.9*	2.2*	1.9	3.3	6.1	4.1	3.2
	Min	0.5	0.5	0.5	0.4	0.3	0.1	0.2	0.3
	Max	43.8	26.5	17.4	76.8	46.0	25.4	18.7	23.2
Vol (ADC < 900) in T2 lesion (cm^3)	Median	2.7	1.8*	1.2*	1.0*	1.7	2.6	1.1	1.5
	Min	0.2	0.2	0.2	0.2	0.1	0.0	0.1	0.1
	Max	25.0	19.9	10.6	39.1	35.2	13.8	9.8	19.2

The asterix denotes circumstances for which the change in values from the baseline (pre-RT) value was significant based upon a Wilcoxon signed rank test.

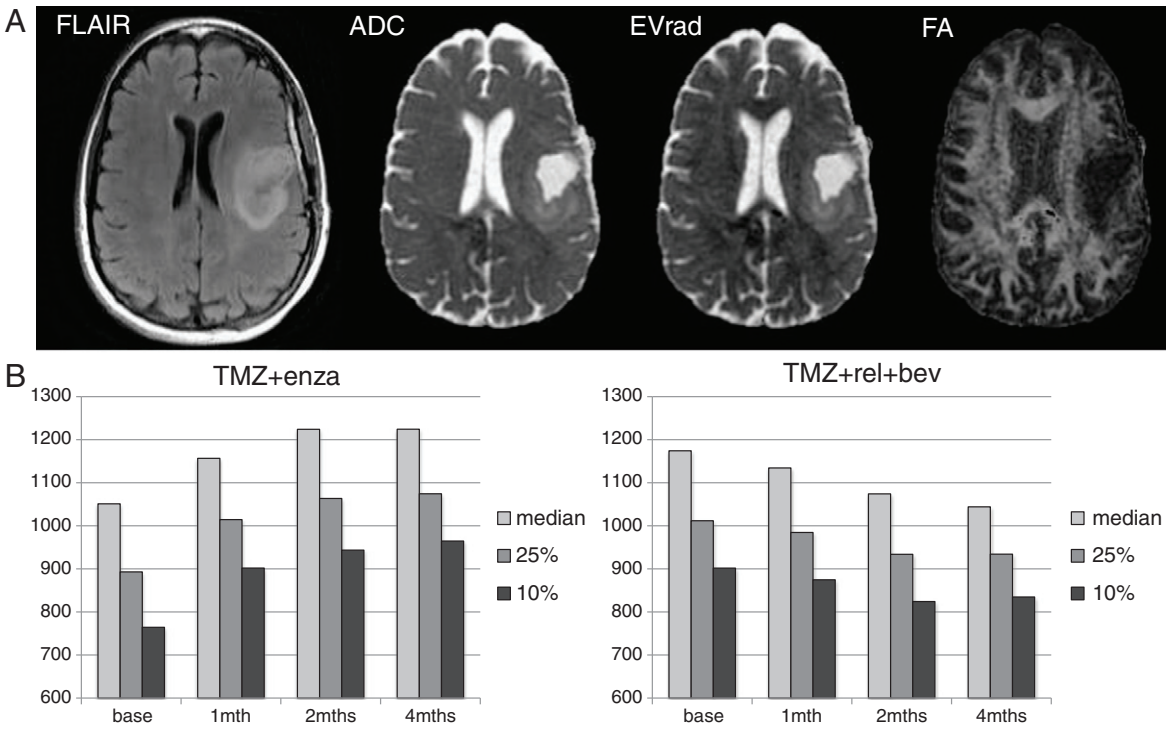

Figure 6. The baseline images (A) from the same patient as shown in Figure 5. FLAIR, ADC, EVrad, and FA. The bar plots in (B) show the time course of changes in ADC histogram percentiles for patients with all four scans. These demonstrate that the ADC increases for the TMZ+enza cohort and show a trend toward decreasing for the TMZ+erl+bev cohort.

were used. For the TMZ+enza cohort, there was a decrease in ADC volume parameters at follow-up examinations, with the change from baseline being significant for all ADC levels at the mid-RT exam, for the volumes with ADC < 1000 and ADC < 900 at the post-RT exam, and for the volumes with ADC < 900 at the 4-month follow-up exam. For the TMZ+erl+bev cohort, only the reduction in volumes in the T2 lesion with ADC < 1200 were significant from baseline to post-RT and from baseline to the 4-month follow-up exam.

Association of Imaging Parameters and Outcome

Table 4 summarizes the Cox proportional hazard analysis of associations between imaging parameters and patient outcomes (PFS and OS) at the baseline and follow-up scans, with the commonly considered clinical factors of age, KPS, and extent of resection being considered as covariates. Clearly, there were more anatomic variables associated with outcome for the TMZ+enza cohort and more diffusion parameters associated with outcome for the TMZ+erl+bev cohort. Of particular note is that the volumes of the T2, CE, and T1S lesion at the 2-month (post-RT) scan were all found to be associated with OS (P = .0012, .0092, and .0099, respectively) and PFS (P = .0076, .016, and .024, respectively) in the TMZ+enza cohort. The only anatomic volume parameters associated with outcome for the TMZ+erl+bev cohort were the CEL at the 1-month scan for OS (P = .039) and at the 2-month scan for PFS (P = .025).

The only diffusion parameters associated with outcome for the TMZ+enza cohort were the volumes of regions with low ADC values at 1-month scan for OS (P = .026) and at 2-month scan for PFS (P = .042). For the TMZ+erl+bev cohort, all of the volumetric diffusion parameters were associated with OS at the 4-month scan with very low P values (P = .000042, .00056, and .0065), whereas the volume with ADC <900 in the T2 lesion was also associated with OS at 1-month (P = .0019) and 2-month (P = .0015) scans. Similar trends were seen for these parameters with PFS, but the significance levels were lower. The time point at which diffusion intensity parameters were associated with outcome was the 2-month scan for OS (P = .007 for ADC and P = .00053 for EVrad) and PFS (P = .0021 for ADC and P = .0011 for EVrad). The 10th percentile values of the ADC and EVrad were also associated with PFS at baseline and 1-month scans.

Table 4. Association of Imaging Parameters with OS and PFS for Patients from the Two Cohorts at Baseline, 1-Month (Mid-RT), 2-Month (Post-RT), and 4-Month (Follow-Up) Scans

Parameter	TMZ+enza								TMZ+bev							
	OS				PFS				OS				PFS			
	Base	1	2	4	Base	1	2	4	Base	1	2	4	Base	1	2	4
T2 volume			X				X	x								
CE volume			X				x			x					x	
T1S volume	x		X				x	x								
Vol (ADC < 1200 in T2L)												X				
Vol (ADC < 1000 in T2L)		x				x						X				x
Vol (ADC < 900 in T2L)		x								X	X	X		x		X
25% ADC in T2L															x	
10% ADC in T2L											X		x	x	X	
25% EVrad in T2L															X	
10% EVrad in T2L											X		x	x	X	

"x" denotes variables that are significant when accounting for age, KPS, and EOR with P < .05, and "X" denotes variables that were significant when accounting for age, KPS, and EOR with P < .01. The diffusion metrics were obtained by analysis of intensities of the ADC and radial diffusivity (EVrad) within the T2 lesion (T2l).

Discussion

This study performed a retrospective analysis of patients who had received advanced MR imaging examinations and had been treated on two different clinical protocols that combined novel therapeutics with involved radiation and TMZ. Although the patients with appropriate imaging data were subsets of the total population in each of the therapeutic trials, their demographics, PFS, and OS were representative of the results from the clinical evaluation of treatment effectiveness [2,3]. In particular, there was a significant difference in PFS between the cohort that received combination therapy with RT, TMZ, erlotinib, and bevacizumab compared with the cohort that received RT, TMZ, and enzastaurin; there was no difference in OS. This observation is consistent with reports from other recent multi-institutional phase III trials of patients with newly diagnosed GBM who received combination therapy that included bevacizumab [4,5]. Factors that may contribute to the prolonged PFS for this patient cohort are changes in permeability of the blood-brain barrier that are expressed by a reduction in the volume of the CE but do not necessarily correspond to a decrease in the number of tumor cells [11]. The latter is commonly referred to as "pseudoresponse" [28,29] and compromises the use of changes in the CE for predicting treatment efficacy [16,30]. Although bevacizumab and enzastaurin are both thought to have an impact upon angiogenesis, their mechanisms of action are different, and it is not surprising that the patterns of changes in imaging parameters are different for the two cohorts.

As a protein kinase C β-inhibitor, enzastaurin is thought to not only impact angiogenesis but also reduce proliferation and increase apoptosis [8,9]. Whereas the link between changes in vessel permeability and contrast-enhanced T1-weighted imaging is well understood, it is not clear how changes in proliferation and apoptosis would be expressed in terms of alterations in imaging parameters. For the cohort of patients treated with enzastaurin, the significant reductions in the volume of the CE and T1S lesions can be directly linked to changes in vessel permeability. Alterations in the volume of T2 lesion were more variable and did not reach statistical significance for the population as a whole. Of interest is that the volumes of all three anatomic lesions that were observed at the 2-month (post-RT) exam were associated with PFS and OS, indicating that there is a direct link between anatomic imaging parameters and tumor burden at this time point.

The increase in ADC and other diffusion parameters that are observed for this cohort of patients at their follow-up scans is consistent with changes in the extracellular environment caused by increased apoptosis, gliosis, and formation of edema. Although these changes do reflect treatment effects, it appears that they act to mask the relationship between ADC and tumor cellularity and result in very few of the diffusion metrics from these time points being associated with outcome. Taken together, the anatomic and diffusion observations suggest that, although there is an effect of enzastaurin on the vessel permeability, the factors that dominate outcome are its antitumor effects on proliferation and apoptosis, which in combination with RT and TMZ are able to directly impact tumor burden.

As a humanized monoclonal VEGF-blocking antibody, bevaziumab has been shown to act on GBM by inhibiting angiogenesis, which has been shown to decrease vascular permeability and reduce the amount of edema through a steroidlike effect [13]. Erlotinib is a tyrosine kinase inhibitor, which acts on epidermal growth factor. When applied in combination with RT and TMZ in a prior clinical trial of patients with newly diagnosed GBM, it was well tolerated but did not confer a survival advantage [2]. Of interest from our study is that, although dramatic early effects of bevacizumab on the volumes of anatomic lesions were clearly seen, there was only a weak association for CEL volume with outcome, and neither the T1S nor T2 lesion volumes were associated with OS or PFS for this patient cohort. This suggests that the early changes in anatomic lesion volumes are secondary effects of the treatments being given and are not representative of changes in tumor burden. Although the reduction in volume of the T2 lesion may have a positive impact on quality of life by reducing the need for additional steroids, it does not appear to prolong survival.

One of the difficulties in using early changes in the volume of the CEL to assess antiangiogenic effects for patients with newly diagnosed GBM is that the volumes considered may be too small to provide reliable parameter estimates. The policy at our institution is to perform maximal safe resection, which means that 30% to 50% of the patients are assessed as having a gross total resection of their enhancing lesion. Although there may be some tumor growth before RT, this means that many of the baseline and follow-up scans either do not enhance or have relatively small enhancing volumes. This problem is accentuated for cases where there are reductions in vessel permeability during treatment. For the cohort treated with bevacizumab in our study, the majority of lesions had a CEL volume at the post-RT exam that was less than 1 cm^3, and a third of the patients had nonenhancing progressive disease. This provides strong motivation for using diffusion imaging parameters to detect biologically relevant changes in the nonenhancing T2.

Parameters that have been proposed as early biomarkers for assessing response to therapy are based upon the histogram analysis of ADC values in the CEL and the manner in which these parameters change before and during treatment [20,21,31] The fDM and its derivatives, such as sfDM maps [32], register serial images and then examine pixel-by-pixel correlations within specific regions of interest for two or more examinations. This has been shown to provide relevant information for evaluation of changes in ADC within the CEL between baseline and 1-month follow-up scans for cases where the overlapping lesion volumes on registered images are greater than 3 mlcc in size. As can be seen from our results, using this cutoff would exclude the majority of our patients from being evaluated. A further issue has been that there is often a large surgical cavity in the baseline exam that shrinks over the next few months and can make it difficult to perform accurate registration between these early scans. Although nonrigid image registration may help to ease this problem [33], the issue of dealing with small lesion volumes still needs to be addressed. For our study, we focused the analysis on variations in diffusion parameters within the relatively larger T2 lesion and did not require the analysis of overlap in serial examinations.

As can be seen from the results from the cohort of patients treated with enzastaurin, the patterns of changes in volumes and diffusion parameters within the T2 lesion are determined by a combination of factors that can make it difficult to interpret whether the treatment has had a positive or negative effect. Infiltrative tumor and vasogenic edema are both commonly present in portions of the lesion but may have opposing effects within the tumor microenvironment [34,35,12]. For tumors that are being treated with bevacizumab, we observed that the anti-VEGF effect leads to more effective control of vasogenic edema, a significant reduction in the volume of the T2 lesion, and a trend toward reduction in ADC and other diffusion values. This is consistent with prior studies of such agents [20,21]. Our results suggest that the reduction in edema observed with

bevacizumab allows there to be a stronger relationship between tumor cellularity and the observed diffusion metrics. This results in a large number of metrics that described low ADC and EVrad values in the T2 lesion being significant risk factors for PFS and OS.

One of the complications in visual interpretation of diffusion images is that many of the metrics highlighted by our analysis correspond to regions within the anatomic lesion that have ADC values of 1000 or less. This means that their intensities on ADC maps are close to the values in normal-appearing white matter and that it may be difficult to make a reliable assessment of tumor boundaries. Defining regions of interest based upon the anatomic lesion, generating histograms of diffusion parameters within the region, and deriving summary statistics that describe the size and shape of the histogram gave objective criteria for assessing response to therapy and predicting survival.

Although the time points and diffusion metrics considered here have strong associations with survival for the patients who were receiving bevacizumab, caution should be taken in interpreting ADC values at other time points. In postoperative images, low ADC values that are due to ischemia effects may be observed. Although these effects typically return to normal within 90 days [36], they may explain why the baseline ADC parameters were not associated with survival in our study. Another issue that can confound the interpretation of low ADC is the formation of gelationous necrosis, which was an indication of response to therapy. This may occur in patients who are treated with bevacizumab but typically not until several months after RT [37–41].

Conclusions

This study evaluated 75 patients with newly diagnosed GBM and found differences in the patterns of early changes in imaging parameters that were associated with the mechanism of action of the agents being given. For patients treated with enzastaurin, the reduction in volume of the CE and T1S lesions, together with the association of post-RT lesion volumes with OS and PFS, suggests that there is a direct impact of the treatment upon tumor burden. This may be due to the antiproliferative effect of enzastaurin itself or to the synergistic effects of RT and TMZ. The situation is more complex for diffusion parameters, as the relationship between tumor cellularity and ADC was confounded by tissue disruption and edema. For patients treated with bevacizumab, the anti-VEGF effect was expressed by reductions in the volumes of the anatomic lesions, but these did not have a direct link with alterations in tumor burden. Despite this observation, the antisteroid effect of bevacizumab was a positive factor in that it appeared to unmask the relationship of diffusion parameters and tumor cellularity. This resulted in metrics such as the volume of regions having low ADC values at follow-up scans and the 10th or 25th percentile of ADC or EVrad values within the T2 lesion being strongly associated with survival. In considering the results obtained from these two patient cohorts, it is clear that interpretation of early changes in the size of anatomic lesions should consider the mechanism of action of the treatment regimen being used and that metrics derived from diffusion imaging can be very helpful in assessing how such changes may impact clinical outcome.

References

[1] Stupp R, Mason WP, van den Bent MJ, Weller M, Fisher B, Taphoorn MJ, Belanger K, Brandes AA, Marosi C, and Bogdahn U, et al (2005). Radiotherapy plus concomitant and adjuvant temozolomide for glioblastoma. *N Engl J Med* **352**, 987–996.

[2] Prados MD, Chang SM, Butowski N, DeBoer R, Parvataneni R, Carliner H, Kabuubi P, Ayers-Ringler J, Rabbitt J, and Page M, et al (2009). Phase II study of erlotinib plus temozolomide during and after radiation therapy in patients with newly diagnosed glioblastoma multiforme or gliosarcoma. *J Clin Oncol* **27**(4), 579–584.

[3] Butowski N, Chang SM, Lamborn KR, Polley MY, Pieper R, Costello JF, Vandenberg S, Parvataneni R, Nicole A, and Sneed PK, et al (2011). Phase II and pharmacogenomics study of enzastaurin plus temozolomide during and following radiation therapy in patients with newly diagnosed glioblastoma multiforme and gliosarcoma. *Neuro Oncol* **13**(12), 1331–1338.

[4] Clarke JL, Molinaro AM, Phillips JJ, Butowski NA, Chang SM, Perry A, Costello JF, Desilva AA, Rabbitt JE, and Prados MD (2014). A single-institution phase II trial of radiation, temozolomide, erlotinib, and bevacizumab for initial treatment of glioblastoma. *Neuro Oncol* **16**(7), 984–990.

[5] Gilbert MR, Dignam JJ, Armstrong TS, Wefel JS, Blumenthal DT, Vogelbaum MA, Colman H, Chakravarti A, Pugh S, and Won M, et al (2014). A randomized trial of bevacizumab for newly diagnosed glioblastoma. *N Engl J Med* **370**, 699–708.

[6] Chinot OL, Wick W, Mason W, Henriksson R, Saran F, Nishikawa R, Carpentier AF, Hoang-Xuan K, Kavan P, and Cernea D, et al (2014). Bevacizumab plus radiotherapy–temozolomide for newly diagnosed glioblastoma. *N Engl J Med* **370**, 709–722.

[7] Clarke JL and Chang SM (2012). Neuroimaging: diagnosis and response assessment in glioblastoma. *Cancer J* **18**(1), 26–31.

[8] Teicher BA, Alvarez E, Menon K, Esterman MA, Considine E, Shih C, and Faul MM, et al (2002). Antiangiogenic effects of a protein kinase Cbeta-selective small molecule. *Cancer Chemother Pharmacol* **49**, 69–77.

[9] Tabatabai G, Frank B, Wick A, Lemke D, von Kürthy G, Obermüller U, Heckl S, Christ G, Weller M, and Wick W (2007). Synergistic antiglioma activity of radiotherapy and enzastaurin. *Ann Neurol* **61**, 153–161.

[10] Senger DR, Galli SJ, Dvorak AM, Perruzzi CA, Harvey VS, and Dvorak HF (1983). Tumor cells secrete a vascular permeability factor that promotes accumulation of ascites fluid. *Science* **219**, 983–985.

[11] Pope WB, Lai A, Nghiemphu P, Mischel P, and Cloughesy TF (2006). MRI in patients with high-grade gliomas treated with bevacizumab and chemotherapy. *Neurology* **66**(8), 1258–1260.

[12] Ananthnarayan S, Bahng J, Roring J, Nghiemphu P, Lai A, Cloughesy T, and Pope WB (2008). Time course of imaging changes of GBM during extended bevacizumab treatment. *J Neurooncol* **88**(3), 339–347.

[13] Friedman HS, Prados MD, Wen PY, Mikkelsen T, Schiff D, Abrey LE, Yung WK, Paleologos N, Nicholas MK, and Jensen R, et al (2009). Bevacizumab alone and in combination with irinotecan in recurrent glioblastoma. *J Clin Oncol* **27**, 4733–4740.

[14] Jain RK, Tong RT, and Munn LL (2007). Effect of vascular normalization by antiangiogenic therapy on interstitial hypertension, peritumor edema, and lymphatic metastasis: insights from a mathematical model. *Cancer Res* **67**, 2729–2735.

[15] de Groot JF, Fuller G, Kumar AJ, Piao Y, Eterovic K, Ji Y, and Conrad CA (2010). Tumor invasion after treatment of glioblastoma with bevacizumab: radiographic and pathologic correlation in humans and mice. *Neuro Oncol* **12**(3), 233–242.

[16] Wen PY, Macdonald DR, Reardon DA, Cloughesy TF, Sorensen AG, Galanis E, Degroot J, Wick W, Gilbert MR, and Lassman AB, et al (2010). Updated response assessment criteria for high-grade gliomas: response assessment in neuro-oncology working group. *J Clin Oncol* **28**, 1963–1972.

[17] Moffat BA, Chenevert TL, Lawrence TS, Meyer CR, Johnson TD, Dong Q, Tsien C, Mukherji S, Quint DJ, and Gebarski SS, et al (2005). Functional diffusion map: a noninvasive MRI biomarker for early stratification of clinical brain tumor response. *Proc Natl Acad Sci U S A* **102**, 5524–5529.

[18] Hamstra DA, Galbán CJ, Meyer CR, Johnson TD, Sundgren PC, Tsien C, Lawrence TS, Junck L, Ross DJ, and Rehemtulla A, et al (2008). Functional diffusion map as an early imaging biomarker for high-grade glioma: correlation with conventional radiologic response and overall survival. *J Clin Oncol* **26**, 3387–3394.

[19] Ellingson BM, Malkin MG, Rand SD, LaViolette PS, Connelly JM, Mueller WM, and Schmainda KM (2011). Volumetric analysis of functional diffusion maps is a predictive imaging biomarker for cytotoxic and anti-angiogenic treatments in malignant gliomas. *J Neurooncol* **102**, 95–103.

[20] Pope WB, Qiao XJ, Kim HJ, Lai A, Nghiemphu P, Xue X, Ellingson BM, Schiff D, Aregawi D, and Cha S, et al (2012). Apparent diffusion coefficient histogram analysis stratifies progression-free and overall survival in patients with recurrent GBM treated with bevacizumab: a multi-center study. *J Neurooncol* **108**, 491–498.

[21] Ellingson BM, Sahebjam S, Kim HJ, Pope WB, Harris RJ, Woodworth DC, Lai A, Nghiemphu PL, Mason WP, and Cloughesy TF (2014). Pretreatment ADC histogram analysis is a predictive imaging biomarker for bevacizumab treatment but not chemotherapy in recurrent glioblastoma. *AJNR Am J Neuroradiol* **35**(4), 673–679.

[22] Ellingson BM, Cloughesy TF, Zaw T, Lai A, Nghiemphu PL, Harris R, Lalezari S, Wagle N, Naeini KM, and Carrillo J, et al (2012). Functional diffusion maps (fDMs) evaluated before and after radiochemotherapy predict progression-free and overall survival in newly diagnosed glioblastoma. *Neuro Oncol* **14**(3), 333–343. http://dx.doi.org/10.1093/neuonc/nor220 Epub 2012 Jan 22.

[23] Macdonald DR, Cascino TL, Schold Jr SC, and Cairncross JG (1990). Response criteria for phase II studies of supratentorial malignant glioma. *J Clin Oncol* **8**, 1277–1280.

[24] Nelson SJ, Nalbandian AB, Proctor E, and Vigneron DB (1994). Registration of images from sequential MR studies of the brain. *J Magn Reson Imaging* **4**, 877–883.

[25] Saraswathy S, Crawford F, and Nelson SJ (2006). Semi-automated segmentation of brain tumor lesions in MR images. 14th Annual Meeting of ISMRM; 2006 [Abstract 1609].

[26] Ellingson BM, Kim HJ, Woodworth DC, Pope WB, Cloughesy JN, Harris RJ, Lai A, Nghiemphu PL, and Cloughesy TF (2014). Recurrent glioblastoma treated with bevacizumab: contrast-enhanced T1 weighted subtraction maps improve tumor delineation and aid prediction of survival in a multicenter clinical trial. *Radiology* **271**(1), 200–210.

[27] Basser PJ and Pierpaoli C (1996). Microstructural and physiological features of tissues elucidated by quantitative-diffusion-tensor MRI. *J Magn Reson B* **111**, 209–219.

[28] Clarke JL and Chang S (2009). Pseudoprogression and pseudoresponse: challenges in brain tumor imaging. *Curr Neurol Neurosci Rep* **9**, 241–246.

[29] Hygino da Cruz Jr LC, Rodriguez I, Domingues RC, Gasparetto EL, and Sorensen AG (2011). Pseudoprogression and pseudoresponse: imaging challenges in the assessment of posttreatment glioma. *AJNR Am J Neuroradiol* **32**(11), 1978–1985.

[30] Reardon DA, Galanis E, DeGroot JF, Cloughesy TF, Wefel JS, Lamborn KR, Lassman AB, Gilbert MR, Sampson JH, and Wick W, et al (2011). Clinical trial end points for high-grade glioma: the evolving landscape. *Neuro Oncol* **13**(3), 353–361.

[31] Khayal IS, Polley MY, Jalbert L, Elkhaled A, Chang SM, Cha S, Butowski NA, and Nelson SJ (2010). Evaluation of diffusion parameters as early biomarkers of disease progression in glioblastoma multiforme. *Neuro Oncol* **12**(9), 908–916.

[32] Ceschin Rafael, Panigrahy Ashok, and Gopalakrishnan Vanathi (2015). sfDM: open-source software for temporal analysis and visualization of brain tumor diffusion MR using serial functional diffusion mapping. *Cancer Inform* **14**(Suppl 2), 1–9.

[33] Boes JL, Hoff BA, Hylton N, Pickles MD, Turnbull LW, Schott AF, Rehemtulla A, Chamberlain R, Lemasson B, and Chenevert TL, et al (2014). Image registration for quantitative parametric response mapping of cancer treatment response. *Transl Oncol* **7**(1), 101–110.

[34] Kono K, Inoue Y, Nakayama K, Shakudo M, Morino M, Ohata K, Wakasa K, and Yamada R (2001). The role of diffusion-weighted imaging in patients with brain tumors. *AJNR Am J Neuroradiol* **22**, 1081–1088.

[35] Guo AC, Cummings TJ, Dash RC, and Provenzale JM (2002). Lymphomas and high-grade astrocytomas: comparison of water diffusibility and histologic characteristics. *Radiology* **224**, 177–183.

[36] Smith JS, Cha S, Mayo MC, McDermott MW, Parsa AT, Chang SM, Dillon WP, and Berger MS (2005). Serial diffusion-weighted magnetic resonance imaging in cases of glioma: distinguishing tumor recurrence from postresection injury. **103**(3), 428–438.

[37] Gerstner ER, Frosch MP, and Batchelor TT (2010). Diffusion magnetic resonance imaging detects pathologically confirmed, nonenhancing tumor progression in a patient with recurrent glioblastoma receiving bevacizumab. *J Clin Oncol* **28**, 91–93.

[38] Rieger J, Bähr O, Müller K, Franz K, Steinbach J, and Hattingen E (2010). Bevacizumab-induced diffusion-restricted lesions in malignant glioma patients. *J Neurooncol* **99**(1), 49–56.

[39] Gupta A, Young RJ, Karimi S, Sood S, Zhang Z, Mo Q, Gutin PH, Holodny AI, and Lassman AB (2011). Isolated diffusion restriction precedes the development of enhancing tumor in a subset of patients with glioblastoma. *AJNR Am J Neuroradiol* **32**, 1301–1306.

[40] Mong S, Ellingson BM, Nghiemphu PL, Kim HJ, Mirsadraei L, Lai A, Yong W, Zaw TM, Cloughesy TF, and Pope WB (2012). Persistent diffusion-restricted lesions in bevacizumab-treated malignant gliomas are associated with improved survival compared with matched controls. *AJNR Am J Neuroradiol* **33**(9), 1763–1770.

[41] LaViolette PS, Mickevicius NJ, Cochran EJ, Rand SD, Connelly J, Bovi JA, Malkin MG, Mueller WM, and Schmainda KM (2014). Precise ex vivo histological validation of heightened cellularity and diffusion-restricted necrosis in regions of dark apparent diffusion coefficient in 7 cases of high-grade glioma. *Neuro Oncol* **16**(12), 1599–1606.